Computation & theory

Check for updates

Anisotropic transport properties of graphene-based conductor materials

Diana Slawig[1], Leo Rizzi[2,3], Tom Rothe[3], Jörg Schuster[3,4], and Christoph Tegenkamp[5,*] (iD)

[1] *Department of Solid State Physics., Leibniz University Hannover, Appelstr. 2, 30167 Hannover, Germany*

[2] *Robert Bosch GmbH, Robert-Bosch-Campus 1, 71272 Renningen, Germany*

[3] *Center for Materials, Architectures and Integration of Nanomembranes (MAIN), Chemnitz University of Technology, 09107 Chemnitz, Germany*

[4] *Fraunhofer Institute for Electronic Nano Systems (ENAS), Technologie-Campus, 09126 Chemnitz, Germany*

[5] *Solid Surface Analysis, Institute of Physics, Chemnitz University of Technology, Reichenhainer Strasse 70, 09126 Chemnitz, Germany*

ABSTRACT

We analyzed nanographite-based materials in a combined study including experimental analysis via 4-point probe STM and simulation to provide a complete picture of microscopic and macroscopic properties of the material. The two- and three-dimensional transport regimes were determined and evaluated regarding the anisotropy of the conductivity. The experimental results yield the full macroscopic conductivity tensor. Microstructural simulations are used to map those macroscopic properties to the microscopic building blocks of the sample. By combining those two, we present a coherent and comprehensive description of the electrical material parameters across several length scales.

Introduction

Since the (re-)discovery of graphene in 2004, there are many activities across different disciplines to transfer its outstanding microscopic properties to macroscopic dimensions. Among others, graphene provides an excellent thermal conductivity [1, 2], a high Young's modulus [3], and a remarkable mobility of charge carriers [4]. Graphene-based conductor materials, such as fibers or films, are promising candidates

that have already shown impressive macroscopic results. Thin films based on graphene nanoflakes are even produced on an industrial scale [5–10]. Nevertheless, the electrical characterization of these materials remains challenging, due to the large geometric anisotropy and an intrinsic inhomogeneity caused by the alignment of the building blocks on the microscale.

The resistivity of a sample ρ is the ratio of an external electric field and the current density. However, this simple relation is only valid for isotropic

Handling Editor: Kevin Jones.

Address correspondence to E-mail: christoph.tegenkamp@physik.tu-chemnitz.de

samples in the diffusive transport regime. In general, the resistivity is a tensor describing the direction-dependent components of the electron conductance in a specific material, which becomes particularly important for composites.

The sample geometry and the overall setup have to be very well known to allow for calculating the resistivity from the resistance. Using 4-point probe (4pp) setups, inherent problems of contact resistances can be overcome, so that the resistance is directly related to the resistivity of a sample. Varying probe distances and geometries further allow access to the transport regimes and the dimensionality of a sample [11, 12]. However, the determination of the resistivity from the resistance becomes more complex if finite size effects and anisotropy come into play. In that case, correction factors for the sample size and for the position of probes with respect to the edges of the sample are mandatory. These factors were extensively evaluated for 2D systems, in many studies and with several mathematical approaches [13–17]. Lately, these factors were also determined for anisotropic and finite samples [13]. However, in 2D systems only the combination of the tensor components can be measured, not the individual components themselves.

Strictly speaking, all this is only valid for homogeneous samples. The determination of the conductivity tensor for an inhomogeneous material is even more complicated and cannot be accessed from the experimental side only. Large-scale fabrication of materials built from microscale elements leads to an inhomogeneity of the material. To characterize the homogeneity, mapping approaches can be used, including characterization via fixed and movable contact and terahertz time-domain spectroscopy [18]. For inhomogeneous and anisotropic materials, simulations are mandatory in order to correlate the microscopic and macroscopic properties. For instance, 1D building blocks such as carbon nanofibers were used to model the properties of 3D macroscopic samples [19–21]. Also, transfer matrix methods for calculating a dynamical conductivity were reported [22]. Very recently, simulations based on random resistor networks were established to model systems made from 2D building blocks [23–25].

In this study, we investigate the transport properties of nanographite-based conductor materials. The determination of the resistivity components via a 4-point probe scanning tunneling microscope (4pp STM) in combination with network simulations provides a complete and coherent picture of microscopic and macroscopic properties of the material and makes it possible to disentangle the conductivity components from each other.

Experimental details

Thin conductive films were synthesized from a liquid graphene dispersion via vacuum filtration. The smallest flakes were eliminated via centrifugation to achieve an average flake size of $2.51 \pm 0.15\ \mu m^2$. The area distribution was obtained from the analysis of scanning electron microscope (SEM) images, as shown in Fig. 1a. More detailed information on the sample production process can be found in Ref. [25].

The thickness of the analyzed sample is $4 \pm 0.3\ \mu m$ and the mass 6.4 mg, which corresponds to a film density of $1.41 \pm 0.11\ g\,cm^{-3}$. The µm-sized flakes are arranged in flat layers and the film is homogeneous on a macroscopic scale. Microscopically, the surface morphology exhibits a certain roughness, as can be seen in SEM shown in Fig. 1b. Due to their random positioning, the individual flakes cause an inhomogeneous structure on the microscale. The dispersion we used was 10 weeks old and therefore the flakes were heavily agglomerated. Due to this agglomeration, the sample is expected to contain nanographite particles rather than monolayer graphene flakes. As we will show below by probe distance-dependent transport measurements, the multilayered nature of these building blocks and their anisotropic assembly shift the expected onset of the 2D regime toward smaller probe distances.

Transport experiments were performed using a 4 tip STM/SEM system, operating at a base pressure of 10^{-8} Pa. Tungsten tips with a diameter of 20 to 80 nm were electrochemically etched and the oxide was removed by applying high voltage pulses under vacuum conditions. The tips can be moved independently via piezomotors, while being observed by SEM and allow a wide range of measurement geometries, i.e., squared arrangement for measuring the anisotropy (cf. inset of Fig. 2, Ref. [13]). The probes were approached fully feedback controlled into tunneling contact, and manually lowered to form an ohmic contact with the sample surface. This ensured reliable transport measurements while
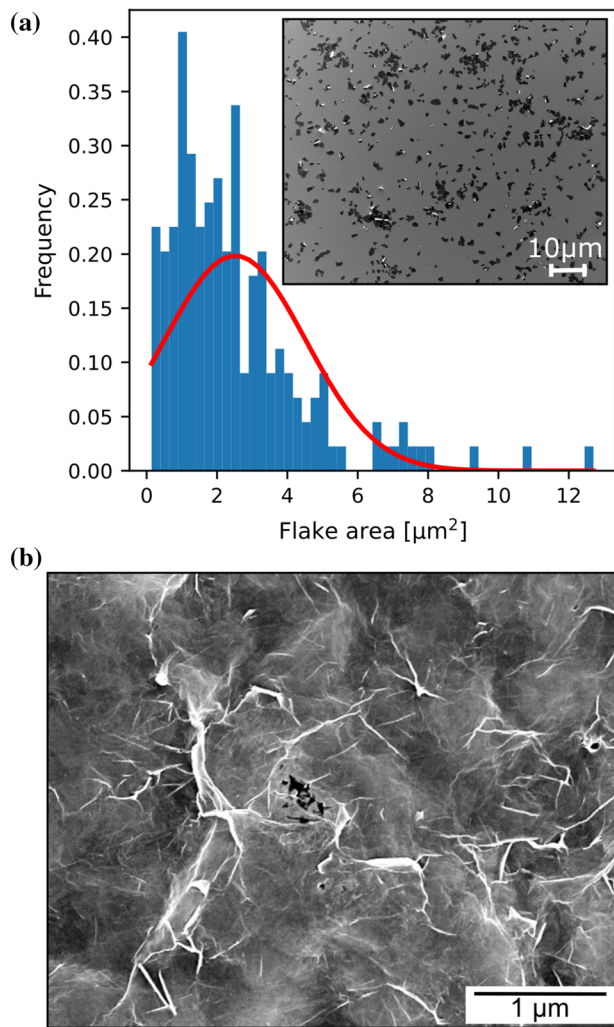
(a)

(b)

Figure 1 **a** Area distribution of graphene flakes on a silicon substrate, determined from a high-resolution SEM image (inset). Around 180 flakes were evaluated with an average flake size of 2.51 ± 0.15 μm^2. **b** SEM image of the sample surface which reveals inhomogeneities on the microscale, while the overall sample is macroscopically homogeneous.

keeping the surface damage reasonably low. To support the microscopic measurements, the sheet resistance was additionally measured via a non-contact eddy current device (SURAGUS EddyCus TF map 2525SR). The resulting spatially resolved measurements visualize the macroscopic homogeneity of the samples.

The simulations are based on a three-dimensional (3D) random resistor network model. Overlaps between flakes constitute the nodes of the network, while the individual flakes connecting the nodes correspond to the edges. In-plane transitions between flakes can be neglected compared to the dominant
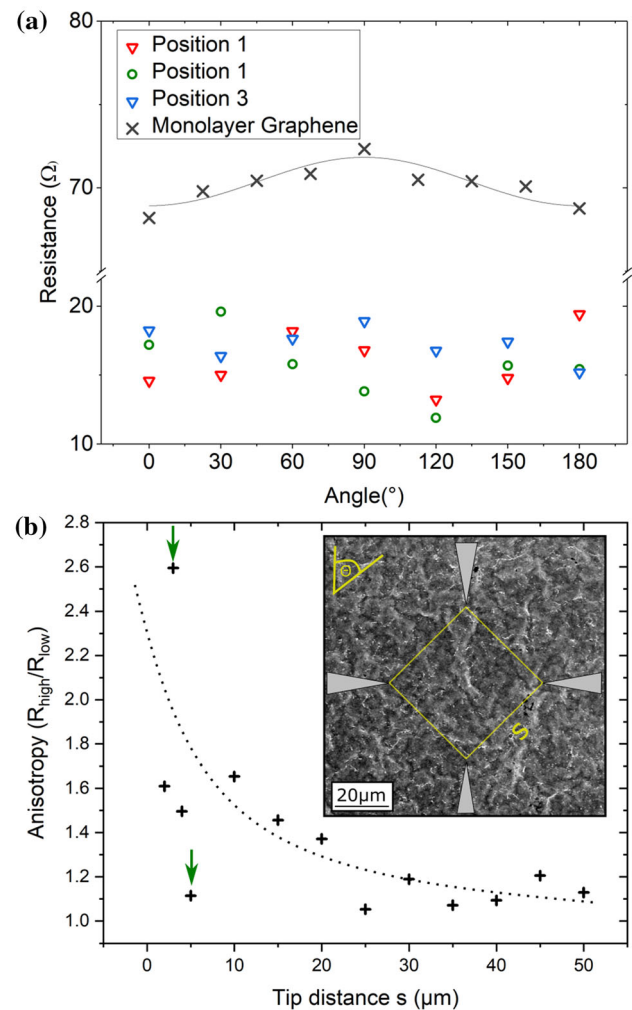
(a)

(b)

Figure 2 **a** Resistance measured at three different positions as a function of the rotation angle (colored symbols) using the so-called rotational square method (fixed probe distance of 50 μm) as depicted in the inset of panel b). For comparison, the data measured on a monolayer graphene sample [26] are shown as well. **b** Resistance anisotropy (R_{high}/R_{low}) as a function of the tip distance. The dashed line is a guide to the eye. The green arrows indicate the strong variation of the anisotropy values. For details, see text. All measurements were taken at 300 K.

out-of-plane transitions. From the fully constructed resistor network, the macroscopic electrical conductivity of the given system is computed. Further details are reported in Refs. [23, 24]. We modeled our nanographite flakes as randomly shaped polygons with a surface area A and a thickness t_{flake}. The individual flakes were grouped into layers, which were then stacked to form a 3D structure. Despite the random flake shapes and positions, we are able to

control the overall packing density of the structure p and the average surface area of the flakes $\bar{A}$.

The resistances of the network edges are based on the following geometric properties: the overlap areas, the distances between overlaps, and the orientation of overlaps toward each other. Additionally, the flake thickness t_{flake}, the in-plane flake conductivity σ_{in} and the conductivity between individual nanographite flakes σ_{out} are included. While the geometric properties are randomly generated and only their averages are controlled, t_{flake}, σ_{in}, and σ_{out} serve as physical input parameters. They characterize the individual microscopic building blocks of the thin film and are closely linked to the macroscopic conductivity tensor. The input parameters can be modeled according to statistical distributions or with uniform effective quantities [23]. Even though the flakes do not form a perfect single layer, this approach has shown to be a good approximation as was shown in comparison with experimental data taken from different films [25].

Experimental results and discussion

After loading the sample to UHV and degassing it, the transport properties were determined with the 4-tip STM/SEM system. First, in order to gain information about the anisotropy, the rotational square method was applied. The tips were arranged in a square configuration, as shown in the inset of Fig. 2b, and subsequently rotated between retract and approach of the tips. The sequential permutation of current and voltage probes allows acquiring data for 180° while rotating the tip assembly by only 90°. The probe distance for this measurement was 50 μm, i.e., large compared to the sample thickness of around 4 μm. Therefore, even the analyzed nanographite-based compound should resemble a 2D material.

The results measured at three different positions across the sample are shown in Fig. 2a. The resistances vary between $R_{high} \approx 20\ \Omega$ and $R_{low} \approx 12\ \Omega$, thus representing the overall good conductivity of this graphene-based conductor material.

For an anisotropic but *homogeneous* 2D material, the anisotropy of the resistances depends on the angle of the injected current with respect to the direction of anisotropy and is uniquely related to the resistivities along the two directions [13, 27]:

$$R\left(\rho_x, \rho_y, \Theta\right) =$$

$$\frac{\sqrt{\rho_x \rho_y}}{2\pi t} \ln \sqrt{\frac{\left(1 + \frac{\rho_y}{\rho_x}\right)^2 - 4\cos^2 \Theta \sin^2 \Theta \left(1 - \frac{\rho_y}{\rho_x}\right)^2}{\left(\sin^2 \Theta + \frac{\rho_y}{\rho_x}\cos^2 \Theta\right)^2}} \quad (1)$$

where t signifies the sample thickness, Θ the angle, and ρ_x and ρ_y the resistivities in x- and y-direction. For comparison, this function is plotted in Fig. 2a together with data obtained for epitaxial monolayer graphene grown on stepped SiC(0001) surfaces [26].

Although there are variations seen upon the change of angle, there is apparently no preferential direction for electron transport. In contrast to the monolayer graphene, but also various metallic chain systems grown by self-assembly on Si-surfaces [28–30], there is no clear maximum visible. Apparently, the situation for this graphene-based conductor material is completely different, and we have to conclude that the uncorrelated variations are explained by microscopic inhomogeneities, i.e., the influence of the exact configuration of the flakes at a certain position.

To shed further light on this effect, we performed probe distance-dependent measurements using a square configuration. Based on the fact that the resistances along different directions show no systematic trends, we used a fixed orientation of the square tip arrangement with respect to the sample. The ratio of the two measured resistance values is used as an indicator for the local anisotropy and the results are plotted in Fig. 2b.

For large tip distances, no significant anisotropy was observed and the ratio is close to 1, i.e., the random arrangement of a high number of flakes averages out any anisotropy. When reducing the tip distance, the anisotropy gradually increases and exhibits a maximum around $s \approx 5$ μm. In this distance range, we also observe strong variations of the anisotropy (marked by arrows). For probe distances on the order of the average flake size (cf. Fig. 1), we expect a vanishing anisotropy. For slightly larger distances, there is a high probability that adjacent flakes are contacted. Thus, the higher anisotropy values on this length scale are indicative for a rotational misalignment of the flakes.

Evidently, for small distances, the number and also the orientation of single nanographitic flakes play a

major role. The random azimuthal orientation of the flakes with respect to the fixed 4-tip assembly explains the conflicting anisotropy values marked by arrows in panel b). For small distances, the exact flake configuration is crucial. We are therefore able to observe a hallmark of the individual flake configuration at a certain position of the sample surface. Based on these conclusions, the sample is made from an anisotropic, microscopically inhomogeneous material.

Besides anisotropy and homogeneity, we consider the dimensionality aspect. As mentioned above, the sample is around 4 μm in thickness, thus for approximately 20 μm probe distance, the corresponding correction factor F_1, taking into account the probe distance s and sample thickness t, is unity. However, $F_1 = 1$ for $t/s < 1/4$ is only valid for homogeneous and isotropic materials, where it marks the 2D regime. In contrast, for $t/s > 4$ the correction factor becomes $F_1 = 2\ln 2(s/t)$, i.e., probe spacing dependent as expected for 3D transport [13, 15].

In order to prove this for the present nanographite-based conductor material, we investigated tip distances from 35 μm up to 300 μm. In this regime, no significant in-plane anisotropy was found, i.e., $\rho_x = \rho_y$. The results are shown in Fig. 3. Clearly, tip distance dependence is found and the 2D/3D transition is visible. However, the transition occurs at larger values, which is due to the nanographitic building blocks as will be explained at a later point. First, the 2D/3D transition is quantified, we made use of resistor network simulations.

As shown above, the system reveals no anisotropy for tip distances larger than $s = 35$ μm and appears as a 2D system for $s > 100$ μm. Therefore, the electrical resistivity in the 2D regime for the squared configuration can be deduced via

$$R_{2D} = \frac{\sqrt{\rho_y \rho_x}}{2\pi t}\ln\left(1 + \frac{\rho_x}{\rho_y}\right) = \rho_{x(y)}\ln(2)(2\pi t)^{-1} \quad (2)$$

where t is the thickness of the sample and ρ_x and ρ_y are the macroscopic resistivities in x- and y-direction [13], which are identical in our case. As a result, the in-plane conductivities $\sigma_{x(y)} = \rho_{x(y)}^{-1}$ for the 2D regime are determined to be $\sigma_x = \sigma_y = 65.2 \pm 1.6$ kS/m.

To substantiate this result, additional macroscopic measurements using the eddy current method were taken, using a pitch of 1 μm and a frequency of 10 MHz. Despite the small pitch, there is an influence
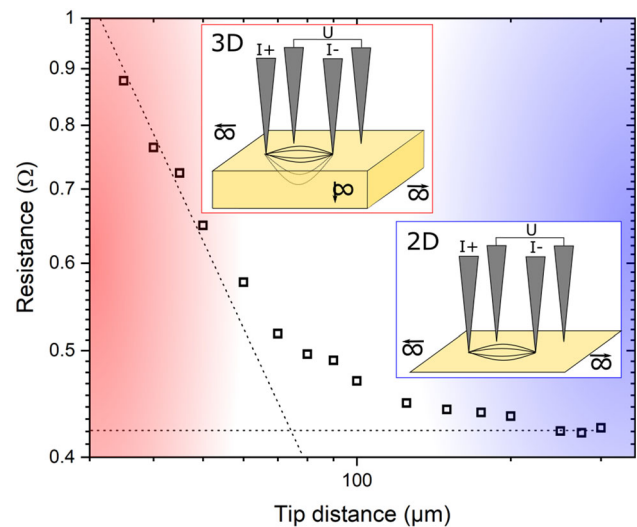

Figure 3 Resistance R versus the 4pp tip distance s. The 2D and 3D regime is indicated in blue and red. The dotted lines describe the expected 2D and 3D behavior based on the extracted conductivity values. The measurements were taken at 300 K using a squared array tip assembly as sketched in the insets.

between neighboring measurement points and the spatial resolution can be approximated to 5 μm. The eddy field penetrates the complete sample at the given frequency, making sure bulk effects are measured. The mean sheet resistance is approximately 4.1 Ω and the resistivity is found to be homogeneous across the sample, as shown in Fig. 4. The resulting conductivity of $\sigma_{eddy} = 61.1$ kS/m matches the microscopic 4pp measurements very well. This underlines the presented data, but only gives insight into the lateral conductance components and cannot fully reveal the anisotropic conductivity tensor including in- and out-of-plane parameters.

For probe separations between $s = 35$-100 μm, we found a 3D behavior (cf. Fig. 3). For this regime, the ρ_z component of the resistivity tensor can be deduced for a square 4pp configuration from [13]

$$R_{3D} = \frac{\sqrt{\rho_x \rho_z}}{\pi s}\left[1 - \left(1 + \frac{\rho_x}{\rho_y}\right)^{-\frac{1}{2}}\right] = \frac{\sqrt{\rho_{x(y)}\rho_z}}{2\pi s}(2 - \sqrt{2}).$$

$$(3)$$

Based on the in-plane conductivity mentioned above, the out-of-plane conductivity is $\sigma_z = 133 \pm 0.5$ S/m. This result clearly corresponds to nanographite rather than graphene [31, 32], which is expected due to the sample preparation method.
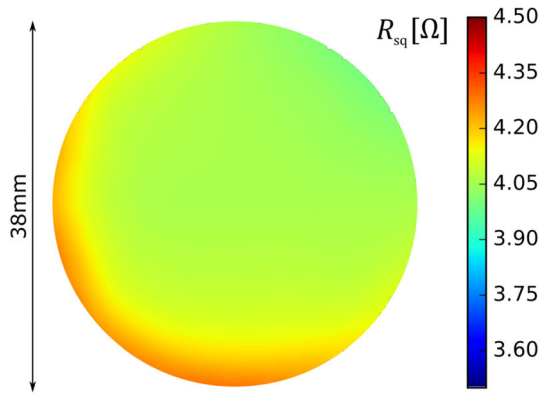
Figure 4 Eddy current measurement of the analyzed film. The sample width diameter is 38 mm. The conductivity appears homogeneous on a macroscopic scale and the average value agrees with the data obtained from microscopic 4pp measurements.

As mentioned above, the 2D/3D transition discussed in context of Fig. 3 occurs at a considerably larger tip separation length than expected for an isotropic sample. However, considering the *effective* thickness of our material $t_{eff} = t\sqrt{\xi}$, with $\xi = \frac{\rho_z}{\rho_{x(y)}} = \frac{\sigma_{x(y)}}{\sigma_z} \approx 490$ as the bulk anisotropy, the condition becomes $s \approx 4t_{eff} = 4t\sqrt{\xi}$. Using the sample thickness of $t=4$ μm and $\sqrt{\xi} \approx 20$, a tip distance of $s \approx 320$ μm is at least required to enter into a full 2D behavior, which is in agreement with our findings.

Simulation

The 4pp transport measurements yield the macroscopic conductivity tensor $\sigma = (\sigma_{x(y)}, \sigma_{y(x)}, \sigma_z)$. With the help of microstructural simulations, we are able to map the macroscopic sample conductivity to the properties of the microscopic building blocks.

For the simulations presented here, the structures comprised a minimum of 95 000 flakes. We fixed the experimentally determined values of $\bar{A} = (2.5 \pm 0.01)$ μm^2 and the packing density $p = 0.6199 \pm 9 \cdot 10^{-5}$ and performed parameter studies for 675 sets of the physical input parameters covering the range of 96 layers $\leq t_{flake} \leq 104$ layers, 100 kS/m $\leq \sigma_{in} \leq 1500$ kS/m and 200 S/m $\leq \sigma_{out} \leq 1000$ S/m. Note that σ_{out} and σ_{in} to out-of and in-plane conductivity components on the microscopic scale, i.e., for our graphitic nanoclusters. These parameter ranges were

identified through considerations of physical limits followed by iterative test simulations. The resulting macroscopic film conductivities $\sigma_{x(y)}$ and σ_z are visualized in Fig. 5.

The flake thickness t_{flake} is directly converted to the number of stacked graphene layers N in each nanographite flake. In this representation, all data points that correspond to a specific flake thickness are located on a straight line, with negligible deviations due to the hidden parameters σ_{in} and σ_{out}. The reason for this is the geometric anisotropy of each individual flake: since the average flake area $\bar{A}$ is fixed, each flake thickness yields a different ratio of the flake dimensions, i.e., a well-defined different geometric anisotropy.

The black frame, magnified in the inset in Fig. 5, indicates the results of the 4pp measurements. The frame immediately shows that the measured results can only be obtained when the average flake thickness in the thin film is between 98 and 104 graphene layers, which confirms the building blocks to be nanographite rather than graphene.

For the best fitting parameter sets compared to the measured conductivity tensor, we generated five different structures each to evaluate the statistical fluctuations due to microstructural variations. The fluctuation was found to be less than 0.5 %, proving the statistical significance of the simulation approach. The mean of each parameter set is shown in Fig. 5.
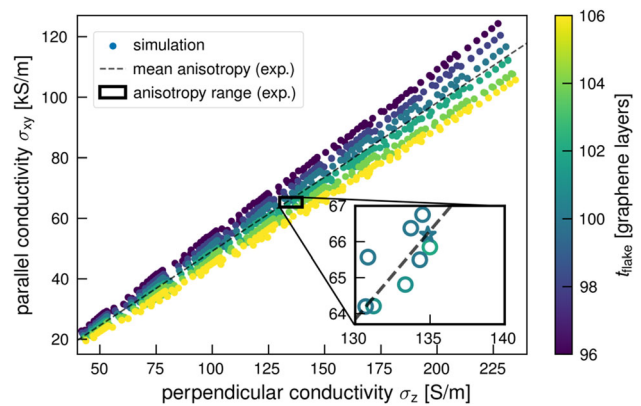

Figure 5 Simulation results for 675 different parameter sets. The black square indicates the anisotropy range expected from the experimental data, the black dotted line the mean experimental anisotropy. The optimized parameters are the in-plane and out-of-plane conductivity values as well as the number of atomic layers in the graphite flakes. The best fitting parameters are indicated by the star in the enlarged part of the simulation results.

Table 1 Best parameters determined by simulation. $\sigma_{\text{in}}, \sigma_{\text{out}}$ are microscopic conductivities while $\sigma_{\text{x(y)}}, \sigma_z$ characterize the macroscopic material

t_{flake} (layers)	σ_{in} (kS/m)	σ_{out} (S/m)	$\sigma_{\text{x(y)}}$ (S/m)	σ_z (S/m)
100	350	810	66.25 ± 0.26	134.86 ± 0.4

While we find several possible combinations of $\sigma_{\text{x(y)}}$ and σ_z that are located within the range of the experimental results, a sweet spot can be identified (green star). The optimal parameter set and the resulting macroscopic thin film conductivities are summarized in Table 1.

The determined values for the flake conductivity $\sigma_{\text{in}} = 350\,\text{kS/m}$ and the conductivity between flakes $\sigma_{\text{out}} = 810\,\text{S/m}$ are well within the known range of graphite conductivities [33]. They complete our microscopic explanation for the macroscopic thin film measurements presented in the previous sections.

Conclusion

We characterized in detail a nanographite-based conductor material with respect to the electrical resistivity. This material is representative for many solid-state phases fabricated from microscopically well-defined two-dimensional building blocks. The systematic variations of probe spacings reveal characteristic length scales at which such compounds can be treated as isotropic and even 2D. Moreover, for length scales close to the size of the microscopic building blocks, details about their assembly were unveiled and used as input for network simulations. By modeling the experimental conductivity values, details of the network structure as well as of the electronic properties of the microscopic flakes became accessible and allowed for a comprehensive description of the material.

Acknowledgements

Funding

Declarations

Conflict of interest The authors declare that they have no conflict of interest.

References

[1] Seol JH, Jo I, Moore AL, Lindsay L, Aitken ZH, Pettes MT, Li X, Yao Z, Huang R, Broido D, Mingo N, Ruoff RS, Shi L (2010) Science 328(5975):213. https://doi.org/10.1126/science.1184014

[2] Balandin AA (2011). Therm Prop Graphene Nanostructured Carbon Mater. https://doi.org/10.1038/nmat3064

[3] Lee C, Wei X, Kysar JW, Hone J (2008) Science 321(5887):385. https://doi.org/10.1126/science.1157996

[4] Du X, Skachko I, Barker A, Andrei EY (2008) Nat Nanotechnol 3(8):491. https://doi.org/10.1038/nnano.2008.199

[5] Stankovich S, Dikin DA, Dommett GH, Kohlhaas KM, Zimney EJ, Stach EA, Piner RD, Nguyen SBT, Ruoff RS (2006) Nature 442(7100):282. https://doi.org/10.1038/nature04969

[6] Stankovich S, Dikin DA, Piner RD, Kohlhaas KA, Kleinhammes A, Jia Y, Wu Y, Nguyen SBT, Ruoff RS (2007) Carbon 45(7):1558. https://doi.org/10.1016/j.carbon.2007.02.034

[7] Xu Z, Gao C (2011) Nat Commun 2(1):1. https://doi.org/10.1038/ncomms1583

[8] Xu Z, Gao C (2015). Graphene Fiber New Trend Carbon Fibers. https://doi.org/10.1016/j.mattod.2015.06.009

[9] Aprojanz J, Dreyer B, Wehr M, Wiegand J, Baringhaus J, Koch J, Renz F, Sindelar R, Tegenkamp C (2017). J Phys Condens Matter. https://doi.org/10.1088/1361-648X/aa9494

[10] Ali AB, Slawig D, Schlosser A, Koch J, Bigall NC, Renz F, Tegenkamp C, Sindelar R (2021) Carbon 172:283

[11] Aprojanz J, Power SR, Bampoulis P, Roche S, Jauho AP, Zandvliet HJW, Zakharov AA, Tegenkamp C (2018) Nat Commun 9(1):4426. https://doi.org/10.1038/s41467-018-06940-5

[12] Aprojanz J, Miccoli I, Baringhaus J, Tegenkamp C (2018). Appl Phys Lett. https://doi.org/10.1063/1.5054393

[13] Miccoli I, Edler F, Pfnür H, Tegenkamp C (2015) J Phys Condens Matter 27:22. https://doi.org/10.1088/0953-8984/27/22/223201

[14] Albers J, Berkowitz HL (1985) J Electrochem Soc 132(10):2453. https://doi.org/10.1149/1.2113598

[15] Zolfaghar Tehrani S, Lim W, Lee L (2012) Measurement 45(3):219

[16] Versnel W (1983) J Appl Phys 54(2):916

[17] Mircea A (1964) J Sci Instrum 41(11):679. https://doi.org/10.1088/0950-7671/41/11/307

[18] Bøggild P, Mackenzie DM, Whelan PR, Petersen DH, Buron JD, Zurutuza A, Gallop J, Hao L, Jepsen PU (2017). Mapp Electr Prop Large Area Graphene. https://doi.org/10.1088/2053-1583/aa8683

[19] Melnikov AV, Shuba M, Lambin P (2018). Phys Rev E. https://doi.org/10.1103/PhysRevE.97.043307

[20] O'Callaghan C, Gomes Da Rocha C, Manning HG, Boland JJ, Ferreira MS (2016) Phys Chem Chem Phys 18(39):27564

[21] Dalmas F, Dendievel R, Chazeau L, Cavaillé JY, Gauthier C (2006) Acta Mater 54(11):2923. https://doi.org/10.1016/j.actamat.2006.02.028

[22] Sasaki KJ (2020). J Phys Soc Jpn. https://doi.org/10.7566/jpsj.89.094706

[23] Rizzi L, Zienert A, Schuster J, Köhne M, Schulz SE (2018) ACS Appl Mater Interfaces 10(49):43088. https://doi.org/10.1021/acsami.8b16361

[24] Rizzi L, Zienert A, Schuster J, Köhne M, Schulz SE (2019) Comput Mater Sci 161:364. https://doi.org/10.1016/j.commatsci.2019.02.022

[25] Rizzi L, Wijaya AF, Palanisamy LV, Schuster J, Köhne M, Schulz SE (2020). Nano Express. https://doi.org/10.1088/2632-959x/abb37a

[26] Momeni Pakdehi D, Schädlich P, Nguyen TTN, Zakharov AA, Wundrack S, Najafidehaghani E, Speck F, Pierz K, Seyller T, Tegenkamp C, Schumacher HW (2020) Adv Funct Mater 30(45):2004695

[27] Kanagawa T, Hobara R, Matsuda I, Tanikawa T, Natori A, Hasegawa S (2003). Phys Rev Lett. https://doi.org/10.1103/PhysRevLett.91.036805

[28] Edler F, Miccoli I, Demuth S, Pfnür H, Wippermann S, Lücke A, Schmidt WG, Tegenkamp C (2015). Phys Rev B Conden Matter Mater Phys. https://doi.org/10.1103/PhysRevB.92.085426

[29] Edler F, Miccoli I, Stöckmann JP, Pfnür H, Braun C, Neufeld S, Sanna S, Schmidt WG, Tegenkamp C (2017). Phys Rev B. https://doi.org/10.1103/PhysRevB.95.125409

[30] Edler F, Miccoli I, Pfnür H, Tegenkamp C (2019). Phys Rev B. https://doi.org/10.1103/PhysRevB.100

[31] Ubbelohde ARJP (1972) Proceedings of the Royal Society of London. A. Mathematical and Physical Sciences 327(1570):289

[32] Banerjee S, Sardar M, Gayathri N, Tyagi AK, Raj B (2005). Phys Rev B. https://doi.org/10.1103/PhysRevB.72.075418

[33] Cermak M, Perez N, Collins M, Bahrami M (2020) Sci Rep 10(1):1. https://doi.org/10.1038/s41598-020-75393-y